Research Article

Journal of Environmental Nanotechnology

Synthesis of NiO/rGO Nanocomposites for Energy Storage Applications through Structural, Optical and Electrochemical Characterization with Machine Learning-based Prediction

V. Anitha[1], Kanimozhiraman[2], S. Senthil Kumaran[3], T. Chitra[4], S. Vinod[5] and A. Jose Anand[6*]

[1]Department of Electronics and Communication Engineering, Sri Muthukumaran Institute of Technology, Chennai, TN, India
[2]Department of Mathematics, SRMIST, E&T, Ramapuram, Chennai, TN, India
[3]Department of Computer Science and Engineering, NPR College of Engineering and Technology, Natham, Dindigul, TN, India
[4]Department of Electronics and Communication Engineering, V.S.B. Engineering College, Karur, TN, India
[5]Department of Electrical and Electronics Engineering, Jerusalem College of Engineering, Pallikaranai, Chennai, TN, India
[6]Department of Electronics and Communication Engineering, KCG College of Technology, Karapakkam, Chennai, TN, India
Received: 07.07.2026 Accepted: 09.08.2026 Published: xx.xx.xxxx
*joseanand97@gmail.com

ABSTRACT

Nickel oxide/reduced graphene oxide (NiO/rGO) nanocomposites have attracted considerable interest as promising electrode materials of high electrical conductivity, tunable electronic structure, and excellent electrochemical characteristics. In this work, a hydrothermal route was employed to synthesize NiO/rGO nanocomposites containing 90 wt.% NiO and 10 wt.% rGO. An intelligent predictive framework integrating fuzzy logic (FL), machine learning (ML), and experimental characterization was developed to optimize the structural, optical, and electrochemical properties of the synthesized material. A Mamdani fuzzy inference system with three input variables (NiO content, rGO loading, and precursor molarity) and three output variables (crystallite size, optical band gap, and photoluminescence (PL) wavelength) was established to estimate material responses. Four ML algorithms, namely Artificial Neural Network, Random Forest, Gaussian Process Regression (GPR), and a Hybrid model were trained using a dataset of 1000 samples with an 80:20 training–testing split to predict crystallite size, optical band gap, PL wavelength, charge storage capacity, charge transfer resistance, energy density, and power density. X-ray diffraction confirmed the formation of crystalline cubic NiO with an average crystallite size of 16.85 nm. Field emission scanning electron microscopy with energy dispersive X-Ray spectroscopy verified the homogeneous distribution of NiO nanoparticles over wrinkled rGO sheets, while Fourier transform infrared analysis confirmed the interaction between NiO and rGO. Photoluminescence analysis revealed an emission wavelength of 430 nm with a band gap of 3.18 eV. The predicted values obtained from FL and ML showed excellent agreement with the experimental measurements, with the Hybrid and GPR models providing the highest prediction accuracy. The proposed integrated experimental–computational methodology offers a reliable and efficient strategy for designing high-performance NiO/rGO nanocomposites for advanced energy-storage applications.

Keywords: Crystallite size; Photoluminescence; Fuzzy logic; Band gap; Machine learning.

1. INTRODUCTION

Recent research has focused extensively on developing high-performance electrode materials that possess high specific capacitance, fast charge transport, high cycling stability, and eco-friendly fabrication process. Nickel oxide (NiO) has been considered as pseudocapacitive material due to high theoretical capacitance, environmentally friendly nature, and rich redox activity, as well as low cost. The major drawbacks of NiO are poor electrical conductivity and instability of its structure during repeated charge–discharge cycles, which make its use difficult in practical applications. To overcome these drawbacks, researchers have studied extensively hybridization approaches with carbon materials, conducting polymers, binary metal oxides, and advanced nanostructured architectures (Arunkumar *et al.* 2026).

Carbon materials prepared from biomass have been of great interest as sustainable support for NiO-based electrodes. The resulting hybrid electrode (wheat straw derived activated carbon, hexagonal boron nitride, NiO and poly(aniline-co-pyrrole)) exhibited excellent electrical conductivity and lower equivalent series resistance while maintaining specific capacitance of 261 F g^{-1}, highlighting benefits of biomass-derived carbon materials in energy storage applications (Ates *et al.* 2025). Likewise, NiO/activated carbon composites were prepared with optimized electrode composition to enhance their charge storage properties in aqueous supercapacitors to achieve high energy density and

charge storage capability (Jublee *et al.* 2025). Similarly, porous carbon/NiO composites were prepared using banana peel as a sustainable biomass and showed a high specific capacitance of 811 F g^{-1} combined with good capability and cycling stability. The porous carbon/NiO composites fabricated from banana peel as a sustainable biomass also showed high specific capacitance of 811 F g^{-1} with excellent rate capability and cycling stability (Al Kiey and Hasanin, 2021).

Enhancing charge transport and electrical conductivity of NiO electrodes using conducting polymers has also been widely utilized to enhance the electrochemical efficiency. The PANI@NiO nanocomposites that were optimized with $FeCl_3$ reached specific capacitance of 971.9 F g^{-1}, demonstrating their effectiveness in creating a composite that is conductive and showed the efficacy of integration of the conductive polymer (Kute *et al.* 2025). Similarly, the NiO/rGO(reduced graphene oxide)/PPy nanocomposites showed a specific capacity of 72.2 mAh g^{-1} and capacitance retention of 88.88% after 10,000 cycles, with the synergistic effect of NiO, rGO and conducting polymers that showcased excellent electrochemical stability (Gayathri *et al.* 2026)**.**

Another approach is to combine NiO with secondary metal oxides to fabricate NiO-based heterostructures with enhanced redox activity and better electron transport. The specific capacitance of NiO–Co_3O_4 nanocomposites obtained by the hydrothermal synthesis method was remarkable at 1466 F g^{-1} (Athira *et al.* 2024). The exceptional capacitance of 1800 F g^{-1} for NiO/ZnO/graphene oxide nanocomposites was due to the synergistic interaction between the three components (Mosaddegh *et al.* 2024). Similarly, scanning electron microscopy (SEM) and Fourier transform infrared (FTIR) analysis results proved that the filler is uniformly distributed with proper adhesion at the interface, and compatibility between the filler and polymer matrix, which led to good structural stability and electrochemical performance (Edlabadkar *et al.* 2026). The porous nanostructure of NiO–ZrO_2 composites contributed to high surface area, which resulted in high value of 248.29 F g^{-1} (Chaudhari *et al.* 2026). The chemically synthesized NiO nanoparticles showed a high capacitance of 174.32 F g^{-1} and retained 96% of capacitance after 2000 cycles, showing that NiO has good electrochemical stability (Devi *et al.* 2026). Moreover, the phase-pure α-$NiMoO_4$ electrodes showed an impressive capacitance of 548 F g^{-1} and an energy density of 79.05 Wh kg^{-1}, highlighting the significance of mixed-metal oxide system performance for high-efficiency supercapacitor electrode (Babu *et al.* 2026). These composite strategies have proven effective time and time again through structural characterization. The successful synthesis of nanocomposites consisting of nickel cobalt oxide and PVA was confirmed by XRD which revealed well-defined crystalline phases of the oxide nanoparticles with excellent structural integrity of the composites (Siwatch *et al.* 2021).

The role of graphene and its derivatives in enhancing the conductivity and electrochemical kinetics of NiO based materials is important (Kalita *et al.* 2021). The rGO has a good conductive network, large number of electroactive sites, and fast electron transport channels, hence it exhibits high rate capability, high capacitance, and high cycling stability in the hybrid electrodes (Raj *et al.* 2025)**.**

Simultaneously, AI and ML methods, as well as statistical optimization methods have emerged as strong tools to speed up the design of materials and prediction of their properties. The mechanical properties of composites reinforced with graphene oxide were well predicted by a multilayer perceptron (MLP) model, with R^2 values of 0.89 and 0.98 for the flexural strength and tensile strength, respectively (Gupta *et al.* 2025). By optimizing the quality of rGO thin film using Levenberg–Marquardt-based MLP, good classification accuracy was achieved (Aminuddin *et al.* 2021). The performance of ZnO/rGO photocatalytic degradation of methylene blue was successfully optimized using a fuzzy inference system (Hir *et al.* 2022). A graph neural network that uses the Transformer architecture was employed to accurately predict battery electrode materials and pinpoint $Na(NiO_2)_2$ as a promising sodium-ion cathode with an R^2 value of 0.82 (He *et al.* 2024). Machine learning has also been proven to predict the long cycling life for NiCo oxide/sulfide hybrid supercapacitors (Teli *et al.* 2026), the linear regression model yielded an R^2 value of 1.000 for electrochemical performance prediction of $NiAgO_2$–rGO electrocatalysts (Iqbal *et al.* 2025). A conductive network of rGO was developed to improve the electron transport ability in the one-pot mechanochemical synthesis of $NiFe_2O_4$@rGO hybrid, which achieved a high specific capacitance of 496 F g^{-1} (1 A g^{-1}) and 93.16% capacitance retention after 5000 cycles in symmetric supercapacitor applications (Ganvir *et al.* 2026).

The NiO/rGO nanocomposites were successfully synthesized through a hydrothermal route, forming the foundation of this investigation. Unlike previous studies, which generally relied on either experimental analysis or computational prediction, the present work integrates machine learning (ML), fuzzy logic (FL), and experimental characterization into a unified framework, enabling faster and more reliable material optimization. The close agreement between the experimental observations and the ML- and FL-based predictions confirms the accuracy and robustness of the proposed methodology for designing energy-storage materials. This integrated strategy provides an efficient approach for developing NiO/rGO nanocomposites with enhanced functional performance. The study focuses on optimizing important material characteristics, including

crystallite size, optical band gap, and charge storage capacity. Hydrothermal synthesis was combined with ML models, namely Artificial Neural Networks (ANN), RF (Random Forest), and Gaussian Process Regression (GPR) and the Hybrid model, together with fuzzy logic simulation to establish accurate predictive relationships. The developed framework also improves electrical conductivity, structural stability, and electrochemical performance while promoting the uniform dispersion of rGO within the nickel oxide matrix. X-ray diffraction (XRD) technique and SEM analysis were employed to examine the crystalline characteristics morphology of synthesized nanocomposites. Thus, the integration of computational intelligence with experimental validation offers a reliable route for developing advanced NiO/rGO nanocomposites suitable for high-performance energy-storage systems and next-generation flexible electronic devices.

2. MATERIALS AND METHODOLOGY

2.1 Materials

Nickel oxide nanoparticles were prepared using nickel nitrate hexahydrate ($Ni(NO_3)_2 \cdot 6H_2O$, Sigma-Aldrich, 99%), sodium hydroxide, and deionized (DI) water as precursor materials. Graphene oxide (GO), which served as the precursor for reduced graphene oxide was synthesized from graphite powder using sulphuric acid, phosphoric acid, potassium permanganate, hydrogen peroxide, ethanol, and DI water. The conversion of GO to rGO was carried out using ascorbic acid as an environmentally friendly reducing agent.

2.2 Synthesis of NiO, rGO and NiO/rGO Nanocomposites

Nickel oxide nanopowder was synthesized through a hydrothermal route. Initially, 0.3 mol/L nickel nitrate hexahydrate (Sigma-Aldrich, 99%) was dissolved in DI water, followed by gradual addition of NaOH solution under continuous magnetic stirring at 60°C. The pH was adjusted to 10–11, leading to the formation of a green $Ni(OH)_2$ precipitate. Stirring was continued for 2–4 hours, after which the suspension was transferred into polytetrafluoroethylene (PTFE)-lined stainless-steel autoclave and maintained at 150–180°C for 12–18 hours. The obtained product was repeatedly rinsed with ethanol and DI water, dried at 80°C for 6–8 hours, and finally calcined in air at 350–400°C for 2–3 hours to obtain crystalline NiO. The calcined material was pulverized using a ceramic mortar and pestle.

Graphene oxide was prepared from graphite powder following the modified Hummers' method (Sameer and Hassan, 2026). A mixed acid solution containing phosphoric acid (85%) and sulphuric acid (98%) in a 9:1 ratio was first prepared and cooled for 2 hours. Subsequently, 4.50 g of graphite was gradually introduced into the acid mixture while continuously stirring. Afterwards, 26.4 g $KMnO_4$ was slowly incorporated, and the reaction mixture was stirred for 14 hours until a dark green suspension was obtained. Hydrogen peroxide (30 wt.%) was then added to remove excess permanganate, and stirring was continued for another 20 hours. The recovered solid was washed thoroughly with ethanol, dried at 90°C for 20 hours, and ground into fine GO nanopowder.

Reduction of GO into rGO was achieved using ascorbic acid as an environmentally friendly reducing agent. GO powder was first dispersed in deionized water (1 mg/mL) and ultrasonicated for 1 hour to obtain a homogeneous suspension. Ascorbic acid was introduced at a 10:1 mass ratio relative to GO, and the mixture was refluxed at 90–95°C for 6–12 hours. The colour change from brown to black confirmed successful reduction. The resulting rGO was isolated by centrifugation, washed several times with ethanol and DI water and dried at 60–80°C.

For fabrication of the NiO/rGO nanocomposites, 2 g NiO and 0.2 g rGO (10 wt.% relative to NiO) were dispersed in equal volumes of deionized water and ethanol using an ultrasonic probe sonicator for 2 hours at ambient temperature. The homogeneous suspension was transferred into PTFE-lined hydrothermal autoclave and treated at 150–180°C for 12–20 hours. After hydrothermal processing, the product was repeatedly centrifuged, dried at 80°C for 8 hours, and finely ground using a ceramic mortar and pestle. The synthesized material was designated as NiO/rGO.

All synthesis procedures employed standardized precursor concentrations and carefully controlled hydrothermal conditions to ensure reproducibility of the prepared nanocomposites (Pore *et al.* 2022). Each experiment was carried out in triplicate. Minor variations among samples may arise from slight changes in precursor concentration, reaction temperature, dispersion of rGO, or instrumental factors such as XRD peak broadening and fluctuations in PL intensity. The complete synthesis procedure is illustrated schematically in Fig. 1.

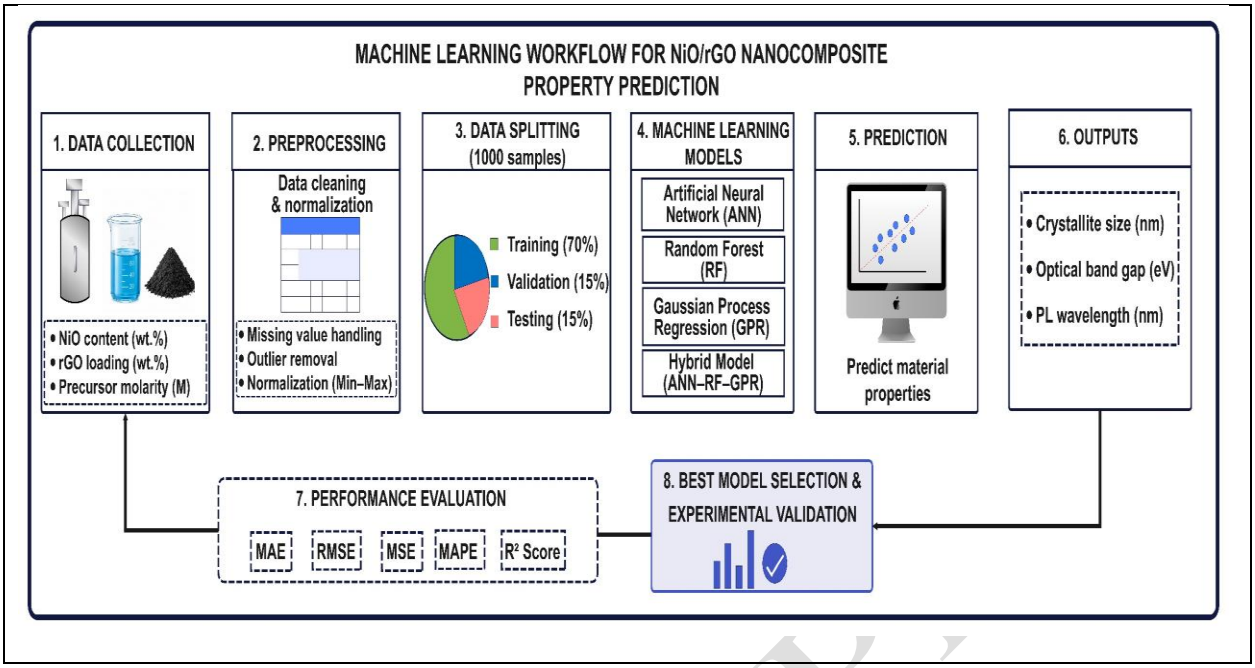

Fig. 1: Schematic synthesis of NiO/rGO

2.3 Characterization Techniques

The synthesized samples were examined by XRD with a Bruker diffractometer. The surface morphology and elemental composition were analyzed by field-emission scanning electron microscopy (FESEM) integrated with energy-dispersive X-ray spectroscopy (EDS) using a Gemini Zeiss instrument operated at an accelerating voltage of 15 kV. Chemical bonding and functional groups of prepared materials were investigated through FTIR spectroscopy.

Spectra were recorded at ambient conditions within 4000–500 cm^{-1} wavenumber region. Optical emission characteristics were evaluated by photoluminescence (PL) spectroscopy on a Horiba Yvon Fluorolog-3 spectrofluorometer fitted with a 450 W xenon arc lamp. Measurements were recorded in steady-state mode over a spectral window of 200–800 nm, enabling detailed assessment of emission behavior and defect-related optical transitions in the synthesized nanocomposites.

2.4 Fuzzy Logic Modeling

A Mamdani-based fuzzy inference framework employing triangular membership functions was established to model structural and optical characteristics of synthesized NiO/rGO nanocomposites. Three process variables associated with material synthesis were considered as input parameters, including NiO concentration, rGO proportion, and precursor solution molarity, since these processing conditions significantly affect particle formation, crystallization behaviour, defect generation, and optical characteristics. Based on the optimized experimental dataset, the operating intervals for the input variables were assigned as 80–100 wt.% NiO, 0–20 wt.% rGO, and 0.20–0.50 M precursor concentration. The corresponding response variables were defined within the ranges of 15–19 nm for crystallite size, 3.0–3.3 eV for band-gap energy, and 415–435 nm for PL emission wavelength.

Every parameter was represented using three fuzzy linguistic categories, namely Low, Medium, and High, described through triangular membership functions. A comprehensive fuzzy rule set was then formulated to capture complex interactions between synthesis variables and resulting material properties (Said *et al.* 2020). The final numerical predictions were generated using the Mamdani reasoning mechanism followed by the centroid defuzzification algorithm, allowing direct validation against both experimentally measured data and machine-learning-based predictions.

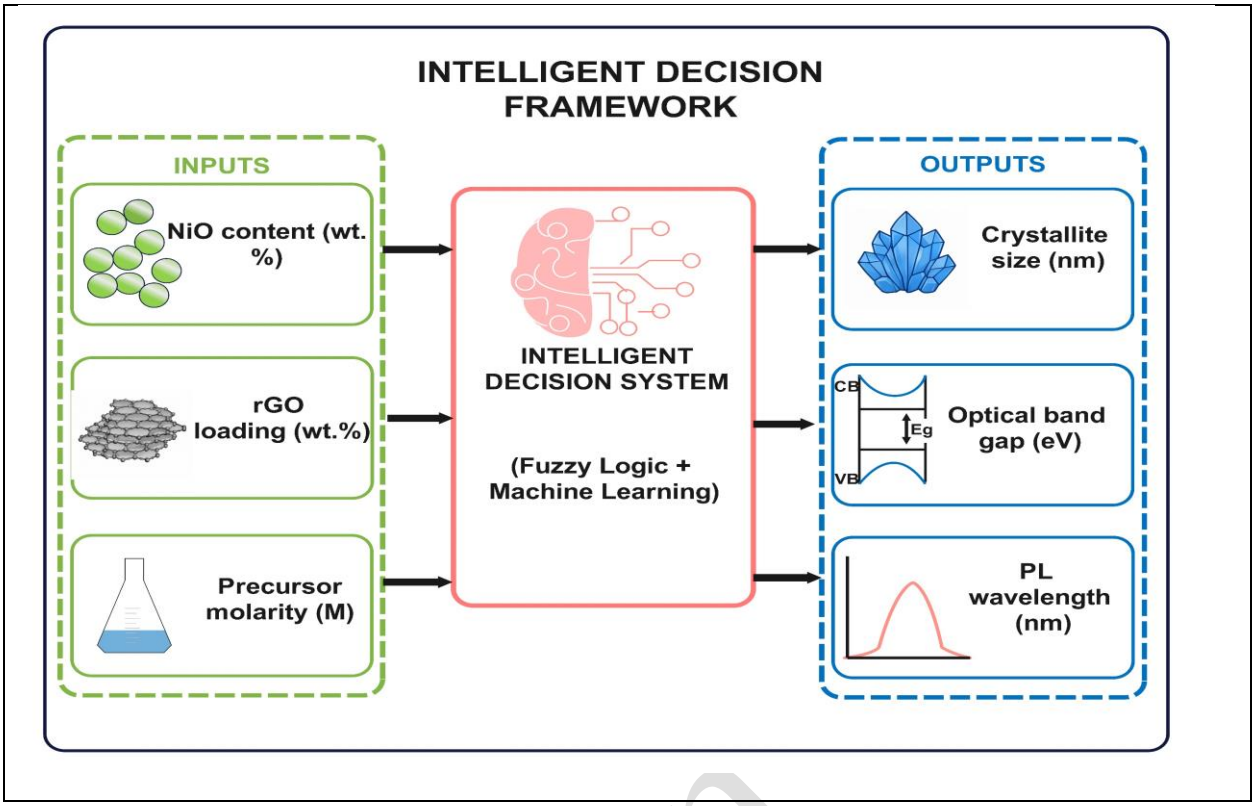

Fig. 2: Intelligent decision framework

2.5 ML Modeling

For evaluation of structural, electrochemical and optical behaviour of the synthesized NiO/rGO nanocomposites, four machine learning algorithms, namely ANN, RF, GPR, and a Hybrid model, were implemented. The developed models were trained to estimate important material properties, including optical band gap, crystallite size, photoluminescence emission wavelength, charge storage capacity, and charge transfer resistance (CTR) (Vijaya *et al.* 2022). A dataset containing 1000 samples was employed with 80% for model training and remaining 20% reserved for testing. Prior to model development, the dataset underwent preprocessing procedures such as normalization, feature scaling, outlier removal, and data validation to improve prediction reliability. Model parameters were optimized through systematic hyperparameter tuning to obtain the best predictive performance. The developed models were evaluated using the mean absolute error (MAE) and coefficient of determination (R^2), which was used to assess prediction accuracy and model robustness (Doan *et al.* 2026).

Architecture of proposed artificial neural network employed in this investigation is illustrated in Fig. 3. The input layer consisted of three synthesis variables, namely NiO content (wt.%), rGO loading (wt.%), and precursor molarity (M), together with selected experimentally measured characteristics, including crystallite size, PL emission wavelength, and formation temperature, which served as predictive descriptors. Hidden layers with nonlinear activation functions were incorporated to capture complex relationships synthesis parameters and material properties. Output layer generated predictions for optical band gap, charge storage capacity, and charge transfer resistance. Network training was carried out using the backpropagation algorithm with the Adam optimization method, while the MSE was adopted as loss function to minimize prediction error and enhance model convergence.

3. RESULTS AND DISCUSSION

3.1 Fuzzy Logic Results

Triangular membership functions developed for the fuzzy inference system are illustrated in Fig. 4. Although each output variable is represented by the same Low–Medium–High linguistic framework, the membership functions are defined over different numerical domains corresponding to the crystallite size, optical band gap, and PL wavelength. This standardized fuzzy representation ensures consistent inference while accommodating distinct physical ranges of each response variable.

The Mamdani fuzzy inference model was employed to predict structural and optical characteristics of NiO/rGO nanocomposites using NiO content (wt.%),

rGO content (wt.%), and precursor molarity as input parameters. The fuzzy rule viewer shows the real-time inference process and the corresponding defuzzified outputs. For an input combination of 90 wt.% NiO, 10 wt.% rGO, and 0.30 M precursor molarity, the model predicted a crystallite size of 16.4 nm, an optical band gap of 3.15 eV, and a PL wavelength of 425 nm.

These values represent the optimized output generated through centroid defuzzification of the Mamdani inference system. Triangular membership functions were assigned to all selected variables using three linguistic classes: Low, Medium, and High.

This arrangement enabled gradual transitions between adjacent fuzzy regions and improved the representation of nonlinear interactions among the synthesis parameters. The membership limits were defined from the dataset, and the fuzzy rule base was configured in the MATLAB Fuzzy Logic Toolbox.

The Mamdani inference system was then used with centroid defuzzification to convert fuzzy responses into crisp numerical outputs for, crystal size, band gap and PL wavelength (Fig. 5 a-c). Fig. 6 a and b show band gap variation and wavelength variation, respectively. Influence of synthesis parameters on the optical characteristics of NiO/rGO nanocomposites was further investigated by two-dimensional fuzzy response plots.

The relationships between NiO content and the predicted optical band gap, together with NiO content and PL wavelength were analyzed to illustrate effect of composition on optical response of material. These response curves are consistent with the experimental observations and provide an effective means of identifying suitable synthesis conditions for energy-storage applications. Furthermore, the fuzzy inference system was employed to optimize synthesis parameters by evaluating their combined influence on structural and optical properties of nanocomposites.

Three-dimensional response surfaces were generated to visualize the interactions between the input variables (NiO content, rGO content, and precursor molarity) and the predicted outputs, including optical band gap, crystallite size, and PL wavelength (Fig. 7 a-d).

The predictions were obtained using a Mamdani fuzzy inference system based on a set of IF–THEN rules and centroid defuzzification. The inference procedure consisted of fuzzification, rule evaluation, aggregation, and defuzzification to generate crisp output values. The predicted results were subsequently validated against the experimental measurements, and the comparison is summarized in Table 1.

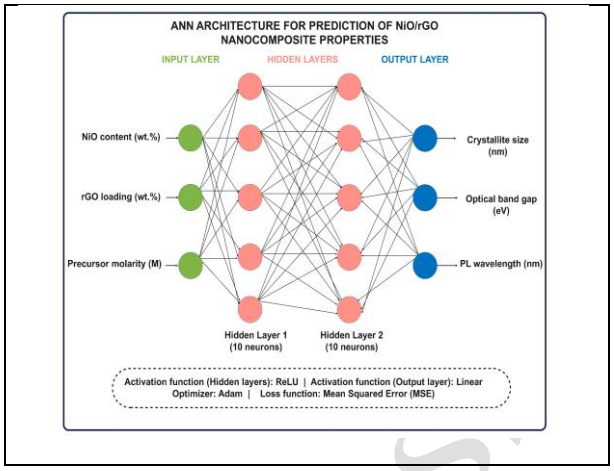

Fig. 3: ANN architecture

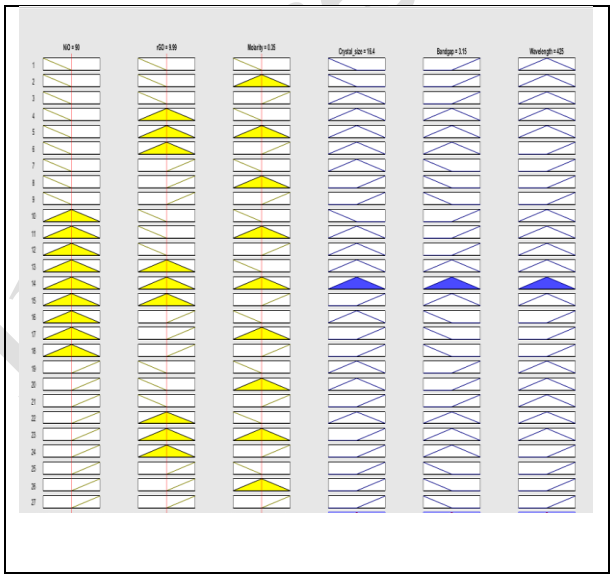

Fig. 4: Fuzzy rule viewer output

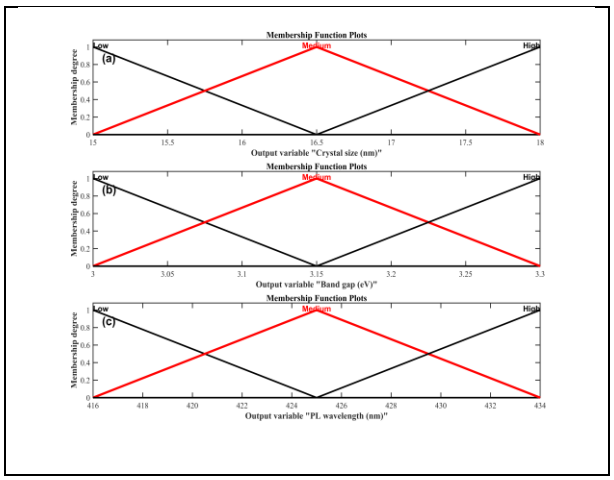

Fig. 5: (a) Crystal size membership function (b) band gap membership function and (c) wavelength membership function

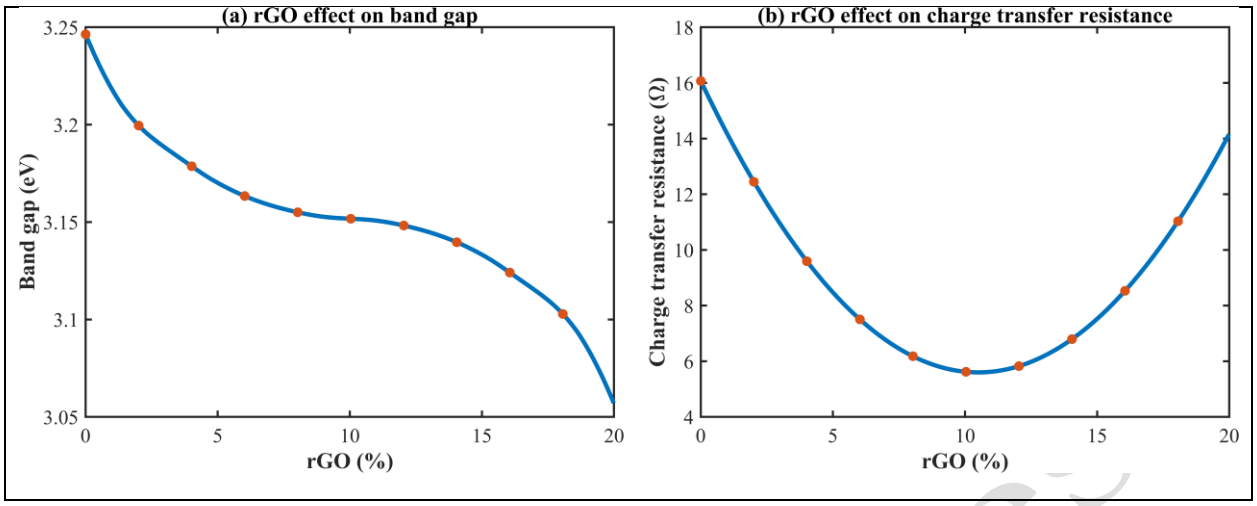

Fig. 6: (a) Band gap variation and (b) Wavelength variation

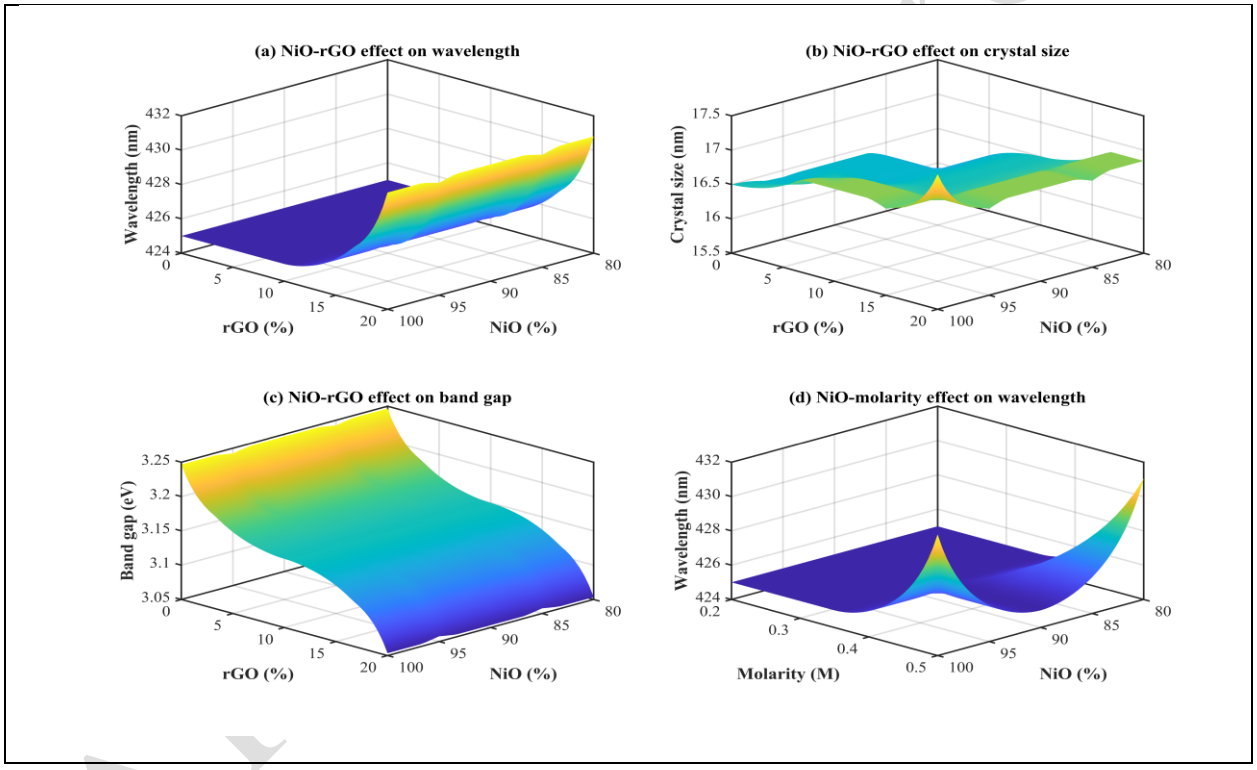

Fig. 7: (a) Wavelength response surface (b) Crystal size response surface and (c) Band gap response surface and (d) Molarity−wavelength response surface

Table 1. Comparison of experimental and fuzzy-predicted values

Parameter	Band Gap (eV)	PL Wavelength (nm)	Crystal Size (nm)
Fuzzy-predicted value	3.13	424.2	16.74
Experimental value	3.18	430	16.85
Relative error (%)	0.97	0.52	0.96

3.2 ML Results

Fig. 8 illustrates the relative contribution of the selected synthesis and structural descriptors toward the prediction of electrochemical performance in the NiO/rGO nanocomposites. The feature-importance analysis indicates that compositional variables and optical–structural parameters play a major role in governing the charge-storage behavior. Among the evaluated inputs, molarity, NiO content, rGO loading, crystallite size, PL wavelength, and formation temperature showed different levels of influence on the predicted response.

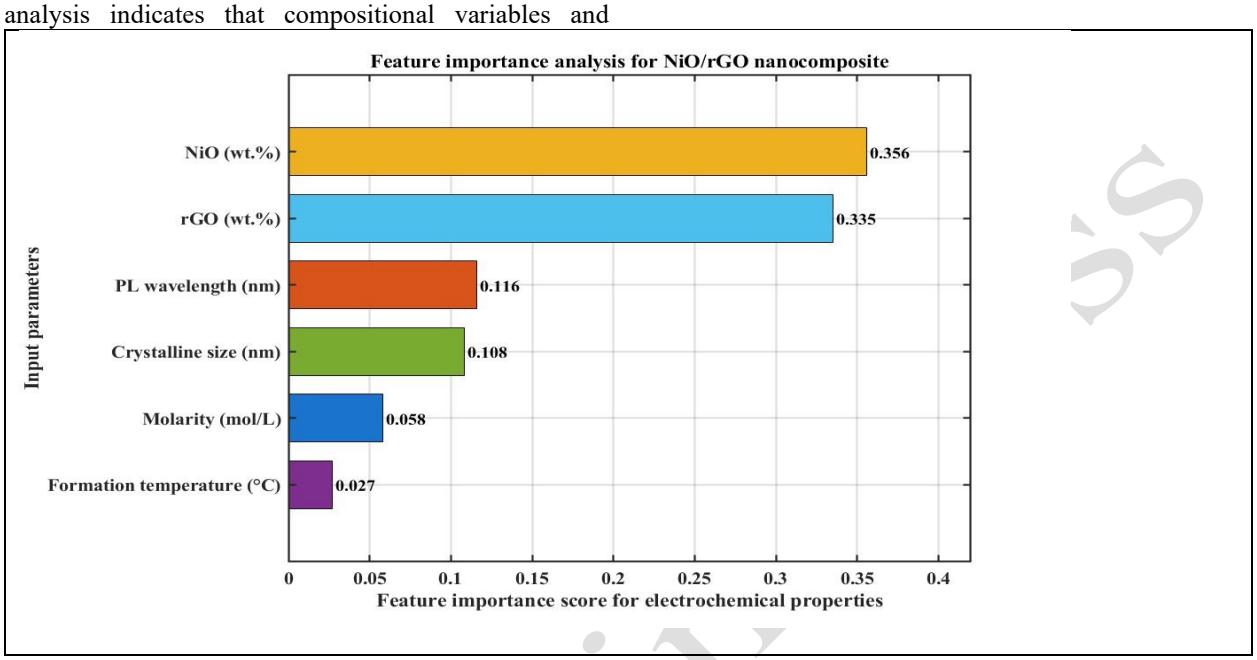

Fig. 8: Feature ranking analysis

Variation in the optical band gap with increasing rGO content is presented in Fig. 9. A continuous reduction in the band gap is observed as the rGO concentration increases, indicating enhanced electronic conductivity and improved charge transport within the NiO/rGO nanocomposites. Band gap lower from approximately 3.4 eV to 2.2 eV as rGO loading increases from 0 to 30 wt.%. This behavior is mainly attributed to the introduction of defect states and stronger electronic interaction between NiO and rGO, which facilitate charge transfer. The tunable optical response demonstrates the suitability of the synthesized nanocomposites for advanced energy-storage. Furthermore, close agreement between the experimental observations and the FL–ML predictions confirms reliability of the developed predictive framework.

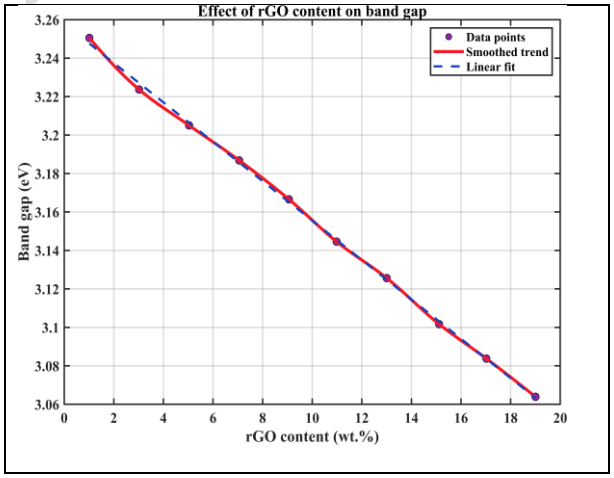

Fig. 9: Band gap versus rGO content

Influence of rGO concentration on charge-transfer resistance is illustrated in Fig. 10. The resistance decreases rapidly from approximately 26 Ω to 5.5 Ω as the rGO content increases to about 10–12 wt.%, reflecting high electrical conductivity provided by rGO. Beyond this composition, the resistance gradually increases and reaches nearly 14 Ω at 29 wt.% rGO. This increase is likely associated with excessive rGO accumulation, which promotes particle agglomeration and partially blocks the electron transport pathways. The nonlinear response obtained from both FL and ML

models accurately reproduces this electrochemical behavior.

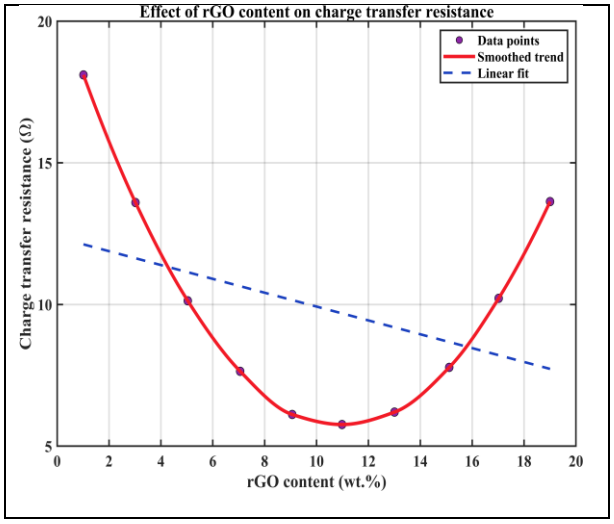

Fig. 10: Charge transfer resistance variation

Effect of formation temperature on optical band gap is presented in Fig. 11. Increasing the formation temperature from approximately 300 °C to 440 °C results in a gradual decrease in band gap from about 3.4 eV to 2.2 eV. This trend suggests that higher thermal treatment improves crystallinity, strengthens interaction between NiO and rGO, and minimizes structural defects, thereby enhancing electrical and optical characteristics of the material. The predicted results obtained from the FL and ML models closely follow the experimental data, confirming their predictive capability. A linear regression model was included as a reference to compare the measured and predicted responses, showing that the data exhibit an overall linear tendency without requiring more complex fitting functions.

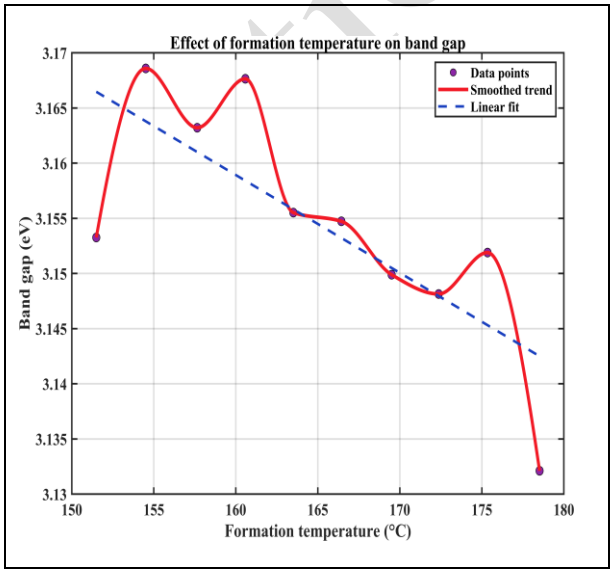

Fig. 11: Thermal and optical correlation

Four models, namely Artificial Neural Network, Random Forest, Gaussian Process Regression, and the proposed Hybrid model, were evaluated by comparing the predicted band gap values with the corresponding experimental measurements (Fig. 12a-d).

The models were developed using the synthesized material parameters as input variables to establish reliable relationships between the processing conditions and the optical response. Close agreement among predicted and measured values confirms effectiveness of all four algorithms in estimating the band gap with high accuracy. Among the evaluated approaches, the Hybrid model produced smallest prediction error and exhibited highest consistency with the experimental results, demonstrating its superior predictive performance.

The integration of machine learning with experimental characterization reduces the need for extensive trial-and-error experimentation, accelerates material optimization, and enhances the reliability of property prediction. Consequently, this data-driven framework provides an efficient strategy for designing NiO/rGO nanocomposites with desired electronic properties for advanced energy-storage applications.

The predictive capability of four machine learning algorithms, namely ANN (Fig. 13a), RF (Fig. 13b), GPR (Fig. 13), and the Hybrid model (Fig. 13d), was evaluated by comparing the estimated and experimentally measured CTR values of NiO/rGO nanocomposites.

The models were trained using synthesized material dataset to accurately predict electrochemical resistance, a key parameter governing charge transport and energy storage performance. Across all four models, the predicted values closely followed the experimental measurements, confirming their strong predictive reliability. Among them, the Hybrid model demonstrated smallest deviation from the measured values over the entire resistance range, indicating superior prediction accuracy and model stability. Likewise, the RF and GPR models provided highly consistent estimations, while the ANN model also achieved satisfactory agreement with the experimental results.

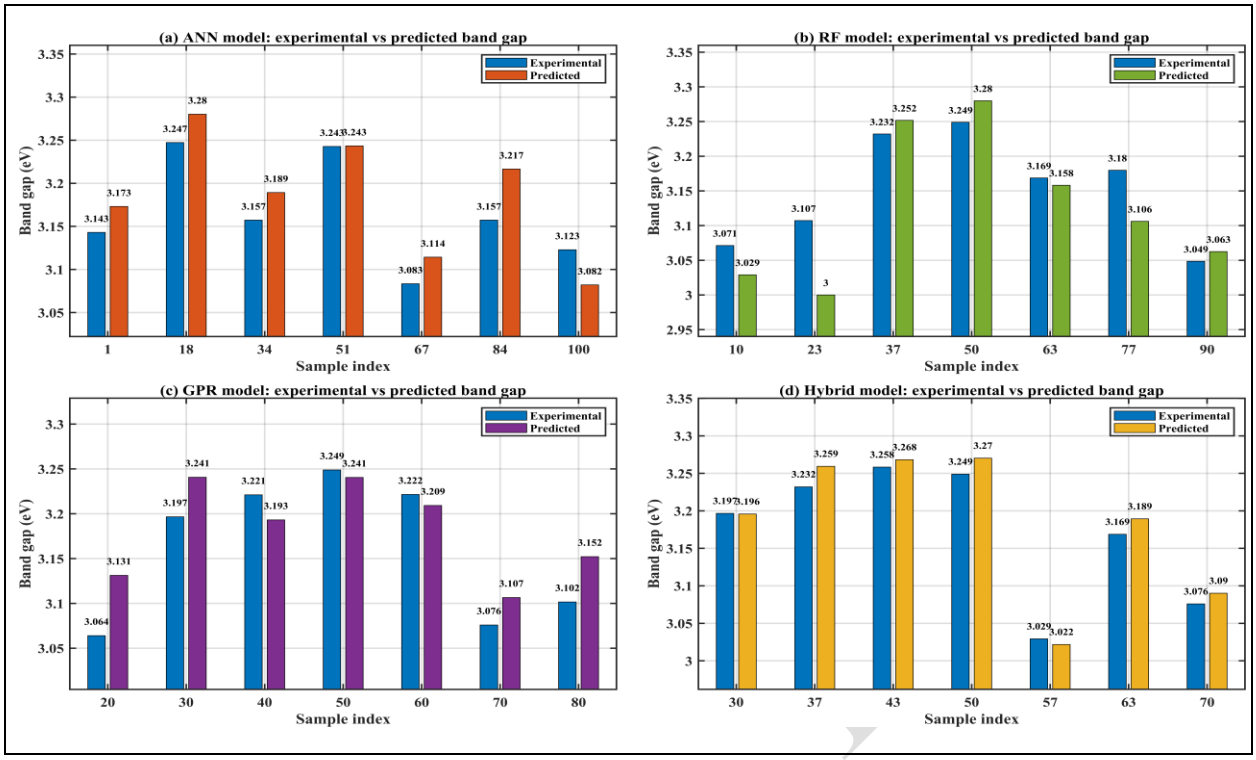

Fig. 12: Band gap prediction of (a) ANN (b) RF (c) GPR and (d) Hybrid model

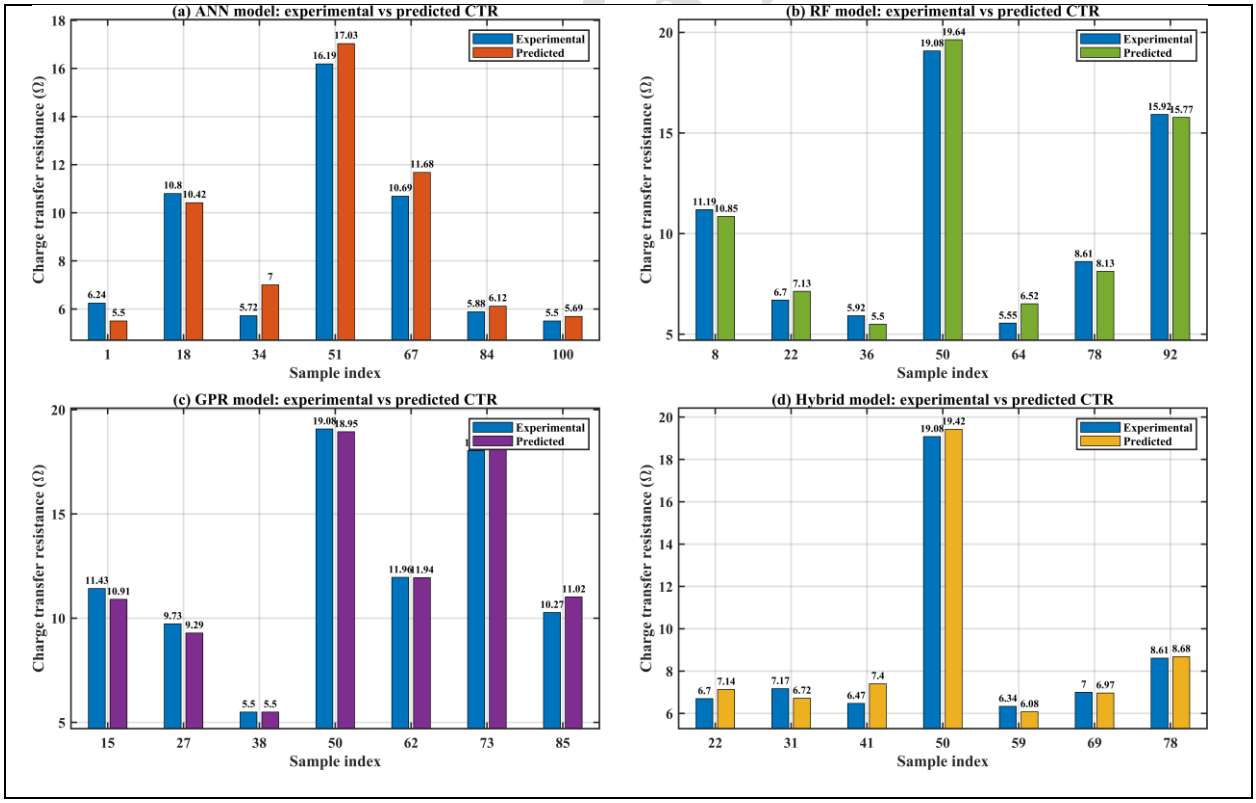

Fig. 13: CTR prediction of (a) ANN (b) RF (c) GPR and (d) Hybrid model

Fig. 14 illustrates the predictive capability of four machine learning approaches, namely ANN, RF, GPR, and the Hybrid model for estimating the key properties of NiO/rGO nanocomposites intended for energy storage applications. The comparison between experimental and predicted band gap values is presented

in Fig. 14a, where all models closely follow the measured trend, while the Hybrid model exhibits the smallest deviation across the selected samples. Fig. 14b compares the experimental and predicted charge storage capacitance values. Although slight variations are observed, the predicted results remain in close agreement with the experimental measurements, with the Hybrid and GPR models providing the highest prediction accuracy. Fig. 14c presents the comparison of CTR, demonstrating that all four algorithms successfully reproduce the experimental behaviour over the entire range. Among them, the Hybrid model consistently provides the closest agreement with the measured data, followed by the GPR model. Overall, the comparison confirms that machine learning can accurately estimate the electrochemical characteristics of NiO/rGO nanocomposites while substantially reducing experimental effort.

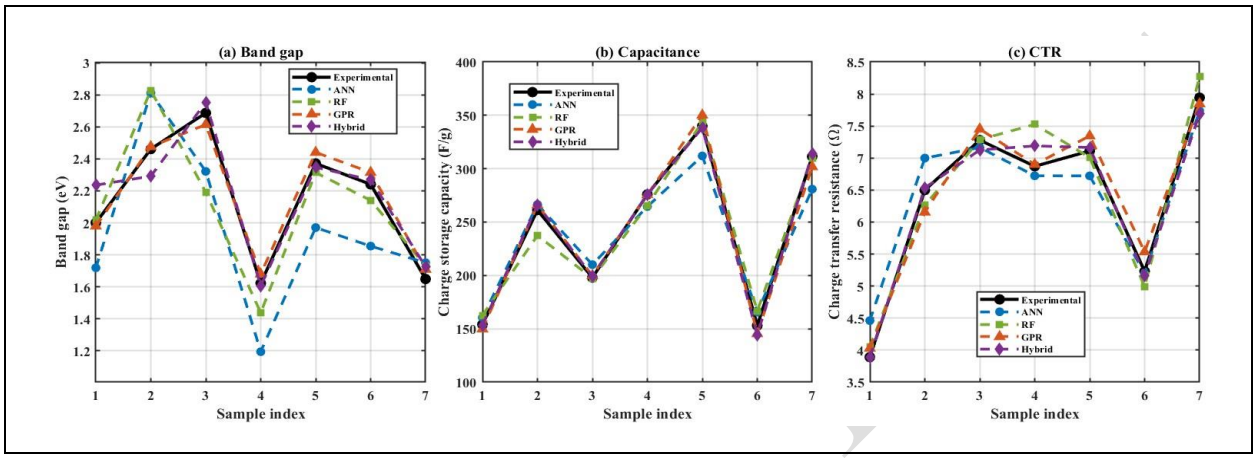

Fig. 14: Experimental and ML comparison

Table 2: Comparative MAE analysis

Property	ANN-MAE	RF_MAE	GPR_MAE	Hybrid-MAE
Band gap	0.225	0.19674	0.068753	0.07812
Charge transfer resistance	0.35791	0.23975	0.22643	0.16325
Charge storage capacity	9.5392	8.1177	7.0212	4.8737

Fig. 15 compares the coefficient of determination (R^2) obtained for the three predicted properties using four machine learning algorithms (ANN, RF, GPR, and the Hybrid model). The evaluated parameters include band gap (eV), charge storage capacity (F/g), and charge transfer resistance (Ω). As illustrated, all models achieve high prediction accuracy with most R^2 values exceeding 0.90, indicating strong agreement between experimental and predicted results. Hybrid model provides the highest R^2 for charge storage capacity and CTR, whereas the GPR model exhibits slightly superior performance for band gap prediction. The comparison demonstrates that GPR and Hybrid algorithms are more effective than ANN and RF in capturing the nonlinear behaviour of NiO/rGO nanocomposites. These findings confirm that machine learning offers reliable and efficient approach for predicting electrochemical properties of advanced nanocomposites used in energy storage applications.

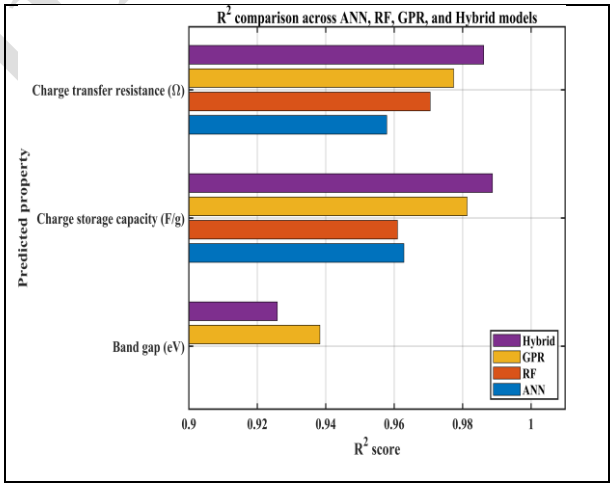

Fig. 15: Regression accuracy comparison

Predictive capability of NiO/rGO nanocomposites, four machine learning algorithms, namely ANN, RF, GPR, and the Hybrid model were employed, and their R^2 values are summarized in Table 3. The high R^2 values obtained for band gap, charge storage capacity, and CTR indicate that these models can effectively estimate the electrical and electrochemical properties of the synthesized nanocomposites. Among the evaluated methods, the Hybrid model achieved the highest prediction accuracy for charge storage capacity (R^2 = 0.98962) and CTR (R^2 = 0.98446), whereas the GPR model provided the best prediction for band gap (R^2 = 0.94182). The hybrid approach demonstrated most

balanced and reliable performance across all predicted properties, while GPR also showed excellent capability in modelling nonlinear relationships. These results confirm that integrating ML algorithms is an effective strategy for optimizing NiO/rGO nanocomposites for advanced energy storage applications. Previous studies have reported fabrication of novel MnO_2/NiO/ZnO trijunction electrode by successive electrochemical deposition for high-performance supercapacitor applications. Electrode achieved specific capacitance of 1569.75 F g^{-1}, while ANN accurately predicted its cyclic voltammetry behavior with an error of less than 0.05%, demonstrating the effectiveness of combining experimental and AI-based approaches for energy storage research (Alimi *et al.* 2022).

Table 3: Comparison of regression performance

Property	ANN $-R^2$	RF $-R^2$	GPR $-R^2$	Hybrid-R^2
Band gap (eV)	0.89389	0.81159	0.94182	0.92523
Charge transfer resistance (Ω)	0.92552	0.96728	0.97059	0.98446
Charge storage capacity (F/g)	0.95714	0.97346	0.98028	0.98962

3.3 Structural and Optical Characterization

3.3.1 XRD Analysis

X-ray diffraction results of the synthesized NiO/rGO nanoparticles with a NiO:rGO ratio of 9:1 (NiO = 90 wt. % and rGO = 10 wt. %) are shown in Fig. 16. The reflections marked as (111), (200), (220), (311) and (222) for cubic NiO were found to be very intense at approximately 36.8°, 43.3°, 62.8°, 76.5° and 80.3° (2θ), respectively, indicating formation of well-crystallized FCC NiO phase. The characteristic (001) diffraction peak corresponding to GO was not observed in the rGO sample, suggesting the successful reduction of GO, which was verified by the presence of a broad diffraction band around 24–26°. This change was because of removal of oxygen containing functional groups and reduction in interlayer spacing after chemical reduction. When present, weak additional reflections near 37.9° and 65.5° are generally believed to be due to incomplete transformation of the precursor and hence are attributed to trace $Ni(OH)_2$. The incorporation results in slight change in NiO crystal lattice due to interactions at the interface, lattice distortion and generation of defects. Oxygen vacancies, residual strain or interface-related structural disorder generated during hydrothermal synthesis result in minor peak broadening or low intensity shoulders. Recent studies revealed that the XRD analysis showed successful incorporation of Cu–Fe into NiO without formation of any secondary phase and achieved the phase-pure $Ni_{0.9}Cu_{0.04}Fe_{0.06}O$. Better crystallinity and structural stability are favorable for the supercapacitor applications of the electrodes (Sivakumar *et al.* 2021).

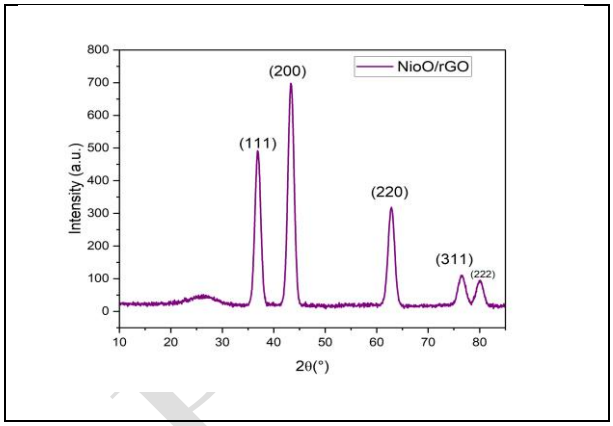

Fig. 16: XRD structural characterization

The degree of structural ordering and crystallinity of the synthesized materials can be obtained through diffraction peak profile. Nanoscale crystallites were formed due to relatively broad diffraction reflections. The crystallite size of NiO/rGO nanocomposites was calculated from most intense (200) diffraction peak by Debye–Scherrer equation and the results are summarized in Table 4. Incorporation of rGO effectively restricted the growth of NiO crystal during the hydrothermal synthesis process, 16.85 nm being the average crystallite size. The decrease in crystallite size observed was attributed to strong NiO nanoparticles-interfacial interactions that hinder agglomeration of NiO nanoparticles and facilitate uniform nucleation. Considering that NiO crystalizes in a face centred cubic (Fm^3m) structure, the interplanar spacing (d) was calculated from the cubic lattice expression $1/d^2 = (h^2 + k^2 + l^2)/a^2$, where h, k and l are the Miller indices and a is the lattice constant. Therefore, the cubic expression was used instead of the equation used for hexagonal crystal systems.

$$\frac{1}{d^2} = \frac{4}{3}\left(\frac{h^2 + hk + k^2}{a^2}\right) + \frac{l^2}{c^2}$$

$$D = \frac{K\lambda}{\beta \cos\theta}$$

Table 4. Structural and optical characteristics

Sample	2θ of (200) Peak (Degree)	Optical Band Gap (eV) by PL	Crystallite Size (nm)	FWHM (Degree)

NiO/rGO	43.30	3.18	16.85	0.50

3.3.2 SEM and EDS Analysis

The synthesized NiO/rGO nanocomposites were analysed by field-emission scanning electron microscopy and the resulting micrograph is shown in Fig. 17a. The image shows that NiO nanoparticles are evenly distributed across the wrinkled rGO nanosheets and tightly bound to them, which suggests a good coupling between the two materials. This hierarchical structure should yield a larger active surface area, better electron transfer and higher electrochemical activity, and hence help to make the composite a potential material for energy storage and photocatalytic applications. The elemental composition was further investigated using energy-dispersive X-ray spectroscopy along with FESEM system operated at 15kV. The EDS spectrum in Fig. 17b confirms presence of carbon, oxygen and nickel, which confirms the formation of the NiO/rGO composite. The measured Ni and O contents are correlated with the expected NiO phase while the relatively high content of carbon was attributed to structure of reduced graphene oxide. Furthermore, the SEM and EDS analysis indicates that NiO nanoparticles are evenly distributed in the rGO matrix without apparent phase segregation. The particle-size distribution is given in Fig. 17c, calculated from the FESEM micrographs and image processing using ImageJ software. The particle size distribution is mostly in the range of 0.1 µm to 2 µm, having an average size of ~ 3.08 µm, thus having a fairly small size distribution. This uniform morphology further supports successful incorporation of NiO onto rGO sheets as well as the structural homogeneity of the synthesized nanocomposites.

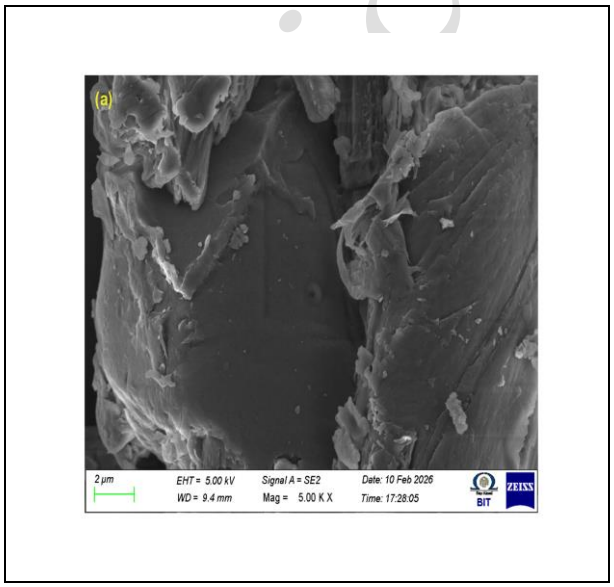

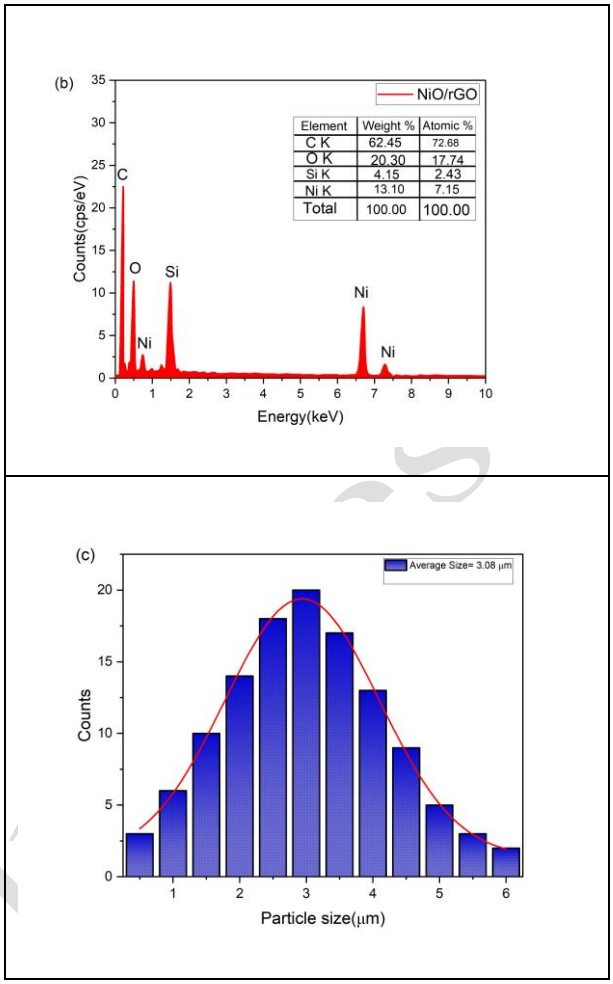

Fig 17: (a) Surface morphology analysis, (b) Elemental composition mapping and (c) Particle size distribution

3.3.3 FTIR Analysis

FTIR spectroscopy was used to identify surface functional groups at the rGO -incorporated nickel oxide (NiO/rGO) nanocomposites. The FTIR analysis of synthesized material showed the characteristic peaks as shown in Fig. 18.

The presence of adsorbed moisture or surface hydroxyl species can be inferred from a broad peak at 3400–3500 cm^{-1}, which corresponds to the stretching vibration of hydroxyl (O–H) groups. The peaks around 1620–1630 cm^{-1} and 1380–1390 cm^{-1} are associated with the carbonyl and hydroxylated carbon absorption modes, which are the residual oxygen-containing species left after the reduction of graphene oxide. The effective reduction of oxygen functionalities during the synthesis process results in a low intensity characteristic band in this region between 1050 and 1100cm^{-1} that is assigned to the stretching vibration of C–O bonds.

A unique absorption band between 520 and 560 cm^{-1} was attributed to Ni–O stretching at low-wavenumber range, thus indicating the successful

synthesis of NiO in the nanocomposites. Oxygen-containing carbon functional groups appear and the Ni-O vibration is observed, revealing successful incorporation of rGO into the nickel oxide matrix and confirming the formation of NiO/rGO nanocomposites. The FTIR spectra showed the characteristic Ni–O stretching vibrations and Ce–O, which confirmed NiO–CeO_2 binary oxide, as reported by researchers at ~460–520 cm^{-1} and Ce–O vibrations at ~540–650 cm^{-1}, respectively. The bands at ~3400 cm^{-1} corresponding to O–H, C=C (~1580–1620 cm^{-1}) and C–N/C=N (~1230–1650 cm^{-1}, for g-C_3N_4), play a vital role in the improvement of the electrode performance during the supercapacitor operation (Balaji *et al.* 2026).

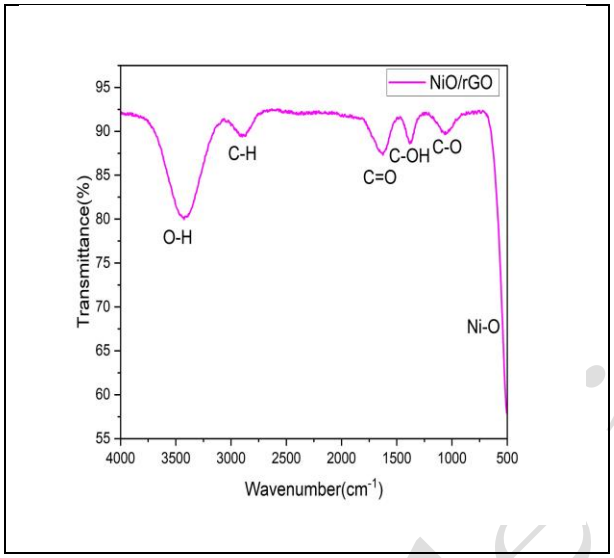

Fig. 18: FTIR spectrum of NiO/rGO nanocomposite

3.3.4 Photoluminescence Spectroscopy

The PL analysis was performed to investigate optical response and defect-related emission behaviour of synthesized NiO/rGO nanocomposites. The PL spectrum (Fig. 19a) shows an emission peak at ~ 430 nm, indicating effective electronic interaction between NiO nanoparticles and rGO. The change in emission wavelength was better separation between recombination of reduced electron–hole and photogenerated charge carriers due to the addition of rGO. Moreover, low emission intensity also implies that the defect-induced recombination centers were suppressed, implying that the charging transport of the rGO network is improved and that the optical performance of the composite is superior. Such properties are desirable in applications where charge migration is required to be efficient, and where electrochemical activity is desired.

The PL results were further used to determine the synthesized nanocomposite's optical band gap energy. The estimated band gap energy was 3.18 eV as shown in the Fig. 19b, which proved that the incorporation of rGO leads to the alteration of the electronic structure of NiO. The nanocomposites showed decreased band gap value than pristine NiO, which may be explained by electronic coupling between NiO and rGO as well as the generation of extra electronic states at the interface between NiO and rGO. The rGO also increases visible light absorption, fosters charge mobility and electron transport throughout the composite structure. The synergistic effects result in better electrical properties, and the synthesized NiO/rGO nanocomposites become attractive energy-storage material for the development of advanced energy-storage devices.

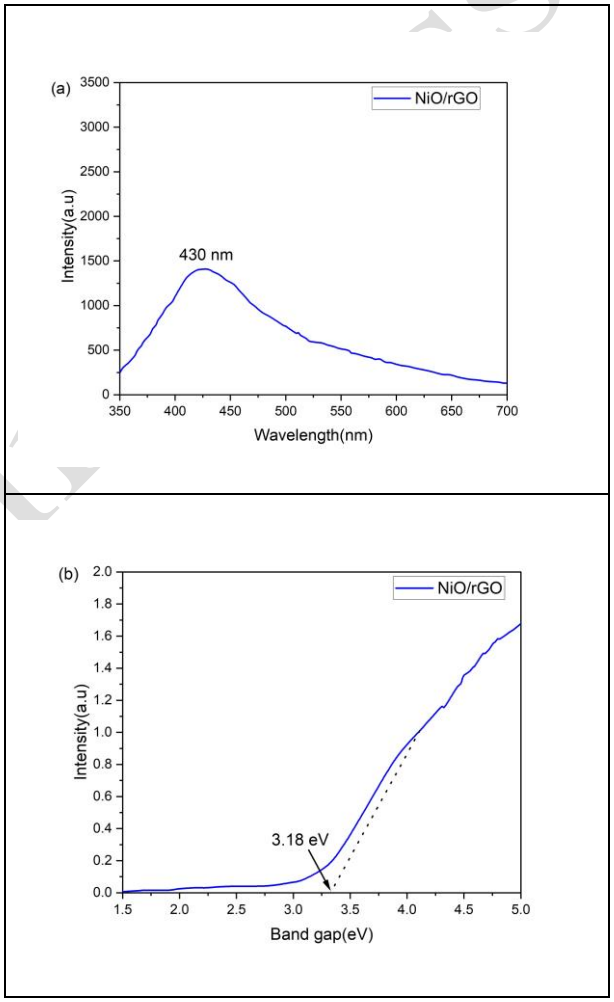

Fig. 19: (a) Photoluminescence emission profile and (b) Band gap determination

The excellent interaction between NiO nanoparticles and conductive rGO network reduces charge carrier recombination and enhances the structural integrity. Therefore, the fabricated nano composite material has excellent ion mobility, electrical conductivity and charge storage capability which is very applicable for advanced supercapacitor and energy storage applications. The combining of rGO gives better physical and electronic properties to the conventional

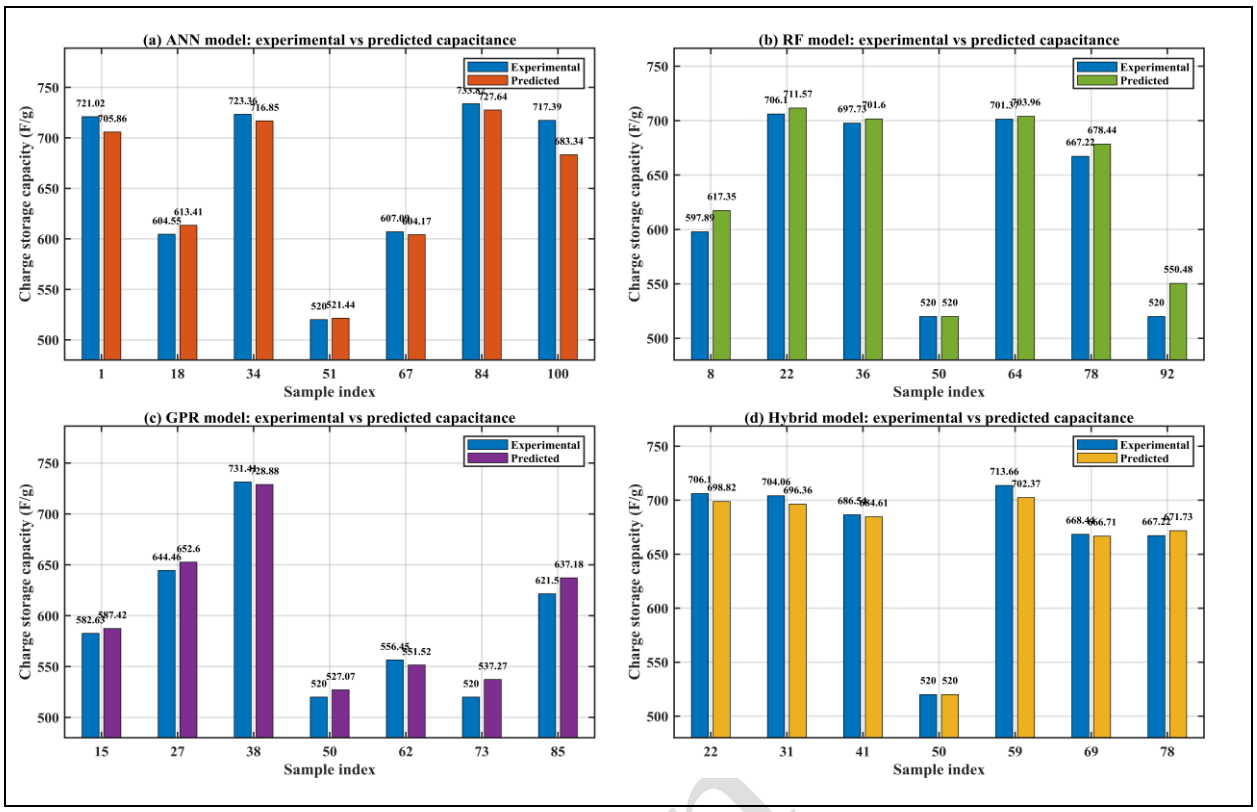

Fig. 20: Charge storage model outputs: (a) ANN; (b) RF; (c) GPR and (d) Hybrid

NiO-based materials, giving a high-performance and environmentally friendly electrode material.

One of the major characteristics of the current research is that it combines experimental characterization, fuzzy logic analysis, and machine learning in a single predictive model. This fusion approach helps determine key material parameters such as crystallite size, optical band gap, photoluminescence wavelength, charge storage capacity, energy density, CTR and charge transfer power density. The present approach has been undertaken unlike previous studies focusing on either experiments or numerical modelling, which shows excellent agreement between the measured results and the predicted results by ANN, RF, GPR and Hybrid model. The good agreement between computations and experimental results validates the robustness of the models developed and suggests an effective way to optimize nanocomposite materials for real applications in energy storage system.

Materials with high energy density, fast charge transport and high cycling durability are desirable for next generation energy devices. The carbonaceous materials in particular, reduced graphene oxide has a large active surface area to increase the interaction between the electrode-electrolyte and to promote fast ion diffusion. Thus, the synthesized NiO/rGO nanocomposite can not only be applied to supercapacitors but also used in other applications such as electrochemical sensors, flexible electronics, nanostructured devices and multifunctional electrode materials. This work is novel because all the mentioned characterization techniques are integrated in acquiring the material properties, which can then be directly compared with the experimental results, through ANN, RF, GPR, Hybrid modelling and fuzzy logic. The methodology is integrated, and provides a path forward to the design of high performance, interpretable nanocomposites while minimizing experimental work.

The electrochemical behaviour is dependent on the amount of rGO, which is a superior conductive material at moderate loading, provides extra electrochemically active sites and improves the electron transport through NiO matrix. But when the rGO content is too high, the sheets agglomerate and partially cover the porous structure, which reduces the diffusion of ions and charge-storage performance. The specific capacitance of the experimental data is compared with the specific capacitance from the ANN, RF, GPR and the Hybrid model in Fig. 20(a–d). The simulated capacitance of all four models are in good agreement with the experimental values, showing the potential to accurately simulate the electrochemical performance with limited experimental efforts. The excellent agreement among experimental

measurements, ML and FL predictions confirms reliability of proposed framework. The trend of the predicted values is consistent with the measured ones, as band gap, crystallite size, CTR, PL wavelength, energy density, charge storage capacity and power density, indicating the success of the developed methodology. In conclusion, the proposed experimental–computational method offers a reliable platform for designing a new generation of NiO/rGO nanocomposites with low internal resistance, high capacitance, optimized electronic properties, and excellent advanced energy-storage technologies.

4. CONCLUSION

A hydrothermal synthesis approach was successfully employed to fabricate NiO/rGO nanocomposites with enhanced structural, optical, and electrochemical characteristics suitable for advanced energy-storage applications. The XRD analysis confirmed formation of crystalline cubic NiO with average crystallite size of 16.85 nm, while FESEM and EDX observations demonstrated the uniform anchoring of NiO nanoparticles on conductive rGO sheets. The FTIR verified the interaction between NiO and rGO, and PL analysis indicated an emission wavelength of 430 nm with an optical band gap of 3.18 eV, demonstrating improved electronic properties after rGO incorporation.

A major contribution of this work is the integration of ML, FL, and experimental characterization into unified material-design framework. A Mamdani fuzzy inference system accurately predicted crystallite size, band gap, and PL wavelength using NiO content, rGO loading, and precursor molarity as input variables. Furthermore, ANN, RF, GPR, and Hybrid machine learning models successfully predicted important electrochemical properties, including charge storage capacity, energy density, charge transfer resistance, and power density. The excellent agreement of predicted and experimental outcomes confirmed robustness and reliability of developed computational models, with Hybrid and GPR models providing the highest predictive performance.

The combined experimental and artificial intelligence framework significantly reduces experimental effort while accelerating material optimization and property prediction. The improved conductivity, enhanced charge transport, reduced charge-transfer resistance, and optimized optical characteristics obtained through rGO incorporation demonstrate the suitability of the synthesized NiO/rGO nanocomposite for supercapacitors and other energy-storage systems. This study establishes a practical data-driven methodology that integrates hydrothermal synthesis, fuzzy logic, advanced characterization, and ML for rapid development of next-generation nanocomposite materials with tailored properties for sustainable energy-storage application.

FUNDING

This research received no specific grant from any funding agency in the public, commercial, or not-for-profit sectors.

CONFLICTS OF INTEREST

The authors declare that there is no conflict of interest.

COPYRIGHT

REFERENCES

Al Kiey, S. A. and Hasanin, M. S., Green and facile synthesis of nickel oxide-porous carbon composite as improved electrochemical electrodes for supercapacitor application from banana peel waste, *Environ. Sci. Pollut. Res.*, 28(47), 66888–66900(2021). https://doi.org/10.1007/s11356-021-15276-5

Alimi, A., Assaker, I. B., Mozaryn, J., Ávila-Brande, D., Castillo-Martínez, E. and Chtourou, R., Electrochemical synthesis of MnO2/NiO/ZnO trijunction coated stainless steel substrate as a supercapacitor electrode and cyclic voltammetry behavior modeling using artificial neural network, *Int. J. Energy Res.*, 46(12), 17163–17179(2022). https://doi.org/10.1002/er.8380

Aminuddin, N. A. B., Ismail, N., Masrie, M. and Badaruddin, S. A. M., Optimization of learning algorithms in multilayer perceptron (MLP) for sheet resistance of reduced graphene oxide thin-film, *Indones. J. Electric. Eng. Comp. Sci.*, 23(2), 686–693(2021). https://doi.org/10.11591/ijeecs.v23.i2.pp686-693

Arunkumar, P., Arulmurugan, B. and Manikandan, M., A sustainable solution to the selection of thermal energy storage materials for concentrated solar power applications and predicted suitable machine learning algorithm, *J. Mater. Res. Technol.*, 41, 5489–5503(2026). https://doi.org/10.1016/j.jmrt.2026.02.124

Ates, M., Yoruk, O. and Bayrak, Y., Correlation between structural properties and electrochemical

performances of h-BN/AC/NiO/Poly(ANI-co-Py) electrodes for supercapacitors, *Ionics,* 32(2), 2091-2110(2025). https://doi.org/10.1007/s11581-025-06891-0

Athira, K., Dhanapandian, S., Suthakaran, S., Dinesh, A. and Ayyar, M., Transition metal oxide-based NiO–Co_3O_4 nanocomposite as an electrode material for the high-performance supercapacitor, *J. Mater. Sci. Mater. Electron.*, 35(17), 1178(2024). https://doi.org/10.1007/s10854-024-12962-1

Babu, N. A. P., Shwetha, K. P. and Renuka, C. G., Structurally optimised α-$NiMoO_4$-based hybrid supercapacitors: Bridging coin cell architecture to real-time prototype device applications, *J. Energy Storage*, 149, 120238(2026). https://doi.org/10.1016/j.est.2025.120238

Balaji, V., Bojarajan, A. K., Sasikaran, R. R., Eswari, K. M., Ponelakkia, D. K., Yuvakkumar, R. and Ravi, G., Synergistic NiO–CeO_2/carbon nanocomposites with long-cycle durability for hybrid supercapacitor applications, *J. Alloys Compds*, 1057(2026). https://doi.org/10.1016/j.jallcom.2026.186747

Chaudhari, N. U., Jagadale, S. K., Shintre, S. N., Patil, R. S., Rathod, M. S., Mhase, P. D., Mandlik, N. T. and Rathod, S. M., Fabrication and electrochemical evaluation of NiO–ZrO_2 nanocomposite electrodes synthesized via sol–gel method for supercapacitor applications, *Mater. Sci. Eng. B*, 331, 119594(2026). https://doi.org/10.1016/j.mseb.2026.119594

Devi, R. R., Thanikaikarasan, S., Devi, N. S., Pachaiappan, R. and Sundaram, K., Facile three-step chemical synthesis of cubic CeO_2 and NiO nanoparticles for efficient energy storage applications, *J. Mater. Sci. Mater. Electron.*, 37(5), 384 (2026). https://doi.org/10.1007/s10854-026-16699-x

Doan, T. D., Nguyen, D. A., Pham, T. H. Y., Luong, D. D., Le, T. T., Thi, N. H., Oanh, H. T., Nguyen, H. T., Thy, P. T. M., Hoang, T. K. D. and Hoang, M. H., High-performance electrochemical sensor based on rGO/FeCo-MOF integrated with machine learning for simultaneous detection of Cd^{2+} and Pb^{2+}, *Talanta*, 310(2026). https://doi.org/10.1016/j.talanta.2026.130105

Edlabadkar, A. P., Chaudhari, S., Harak, S. S., Vijayakumar, M., Nanthakumar, S. and Mayakannan, S., Optimising Tensile and Impact Strength of Polyethylene-based Nanocomposites with Graphene, Carbon and Hemp Fibers, *Int. J. Veh. Struct. Syst.*, 18(1), 39–46(2026). https://doi.org/10.4273/ijvss.18.1.08

Ganvir, V. Y., Alvi, S. N. A., Musrif, P. G., Vadivel, M., Kumar, P. S. and Ulloa, N., Sustainable Mechanochemical Fabrication of $NiFe_2O_4$@rGO Conductive Hybrid for Energy Storage and Environmental Remediation, *J. Environ. Nanotechnol.*, 15(1), 478–491(2026). https://doi.org/10.13074/jent.2026.03.2541991

Gayathri, T., Magray, T., Kavitha, B., Nirmala, M. and Sarawade, P., Tuning NiO/RGO nano-composite electrodes: The synergistic role of polyaniline and polypyrrole in structure, morphology, and charge storage dynamics in supercapacitors, *J. Energy Storage*, 162, 122061(2026). https://doi.org/10.1016/j.est.2026.122061

Gupta, R. K., Langote, V. B., Raj, M. S., Tonk, A., Nanthakumar, S., Suneetha, E. and Mayakannan, S., Performance Evaluation and MLP Prediction of Flax- and Graphene Oxide-reinforced Polyester Composites, *J. Environ. Nanotechnol.*, 14(4), 81–91(2025). https://doi.org/10.13074/jent.2025.12.2531662

He, X., Chen, Y., Wang, S. and Zhang, G., Employing Graph Neural Networks for Predicting Electrode Average Voltages and Screening High-Voltage Sodium Cathode Materials, *ACS Appl. Mater. Interf.*, 16(19), 24494–24501(2024). https://doi.org/10.1021/acsami.4c00624

Hir, Z. A. M., Nik Badrul Alam, N. M. F. H., Shaari, A. S. and Rafaie, H. A., One-Pot Sol-Gel Synthesis of a Zinc Oxide-Reduced Graphene Oxide Composite: Photocatalysis and Kinetics Studies using a Fuzzy Inference System, *Malaysian J. Chem.*, 24(2), 37–46(2022).

Iqbal, S., Aftab, K., Ali Khan, M., Khan, M. R., Javed, N., Jannat, F. T., Ahmad, N. and Hussain, M., Evaluating silver nickelate-reduced graphene oxide for water splitting: A machine learning approach, *Int. J. Hydrogen Energy*, 174, 151403(2025). https://doi.org/10.1016/j.ijhydene.2025.151403

Jublee, J. I., Farm, Y. Y., Rajin, M., Ismail, M. A., Bakri, S. N. S., Makmud, M. Z. H. and Zhu, C., Enhanced Supercapacitor Performance with Nickel Oxide and Activated Carbon Composites in Water-In-Salt Electrolyte (Wise), *Malaysian J. Micros.*, 21(1), 58–66(2025).

Kalita, C., Sarkar, R. D., Verma, V., Bharadwaj, S. K., Kalita, M. C., Boruah, P. K., Das, M. R. and Saikia, P., Bayesian Modeling Coherenced Green Synthesis of NiO Nanoparticles Using Camellia sinensis for Efficient Antimicrobial Activity, *BioNanoSci.*, 11(3), 825–837(2021). https://doi.org/10.1007/s12668-021-00882-x

Kute, S., Zate, M. and Pandey, M., Synthesis and Electrochemical Characterization of APS/$FeCl_3$-PANI@NiO Nanocomposites for Supercapacitors, *Top. Catal.*, (2025). https://doi.org/10.1007/s11244-025-02247-0

Mosaddegh, F., Esfandian, H. and Lashkenari, M. S., Synthesis of NiO/ZnO/GO nanocomposites derived from Ni-Zn-H2BDC metal−organic framework for high-performance supercapacitor electrodes, *Electrochimica Acta*, 502, 144860(2024). https://doi.org/10.1016/j.electacta.2024.144860

Pore, O. C., Fulari, A. V, Parale, V. G., Park, H. H., Shejwal, R. V, Fulari, V. J. and Lohar, G. M., Facile hydrothermal synthesis of NiO/rGO nanocomposite

electrodes for supercapacitor and nonenzymatic glucose biosensing application, *J. Porous Mater.*, 29(6), 1991–2001(2022). https://doi.org/10.1007/s10934-022-01313-2

Raj, M. S., Karthick, K., Arunbharathi, R., Thangavel, C., Ananth, S., Prakash, N. N. and Mayakannan, S., Enhancing Mechanical Properties of Polyethylene-Based Nanocomposites using Graphene Nanosheets, Jute Fiber and Polyethylene-Grafted Maleic Anhydride: An RSM Approach, *Int. J. Veh. Struct. Syst.*, 17(5), 920–928(2025). https://doi.org/10.4273/ijvss.17.5.30

Said, Z., Abdelkareem, M. A., Rezk, H., Nassef, A. M. and Atwany, H. Z., Stability, thermophysical and electrical properties of synthesized carbon nanofiber and reduced-graphene oxide-based nanofluids and their hybrid along with fuzzy modeling approach, *Powder Technol.*, 364, 795–809(2020). https://doi.org/10.1016/j.powtec.2020.02.026

Sameer, A. K. and Hassan, E. K., Manufacturing and Improving Reduced Graphene Oxide (rGO) Membranes for Use as Highly Sensitive Humidity Sensors Based on the Mechanism of Proton Conductivity, *Sens. Imaging*, 27(1), 28(2026). https://doi.org/10.1007/s11220-026-00719-5

Sivakumar, S., Mala, N. A., Batoo, K. M. and Ijaz, M. F., Conserved crystal phase and morphology: Electrochemical supremacy of copper (Cu) and iron (Fe) dual-doped nickel oxide and its supercapacitor applications, *Inorg. Chem. Commun.*, 134, 108959(2021). https://doi.org/10.1016/j.inoche.2021.108959

Siwatch, P., Sharma, K., Manyani, N., Kang, J. and Tripathi, S. K., Characterization of nanostructured nickel cobalt oxide-polyvinyl alcohol composite films for supercapacitor application, *J. Alloys Compds*, 872, 159409(2021). https://doi.org/10.1016/j.jallcom.2021.159409

Teli, A. M., Beknalkar, S. A., Velhal, N. B., Amate, R. U., Morankar, P. J., Dhavale, R. P., Dongale, T. D., Kim, H. and Shin, J. C., Boosting energy storage performance via electron pathway modulation in hierarchical NiCo oxide-sulphide hybrids, *J. Alloys Compds*, 1059, 187060(2026). https://doi.org/10.1016/j.jallcom.2026.187060

Vijaya, P. G., Usha, K. S., Karuppaiah, M., Ravi, G. and Krishnan, P., Fabrication of heterostructure NiO/ZnO thin film for pseudocapacitor application, *J. Sol-Gel Sci. Technol.*, 104(1), 198–210(2022). https://doi.org/10.1007/s10971-022-05919-5